5-6-2017

Calibration of CR-39 Nuclear Track Detectors with Alpha-Particles and Protons for a Measurement of Neutron Interactions with 7Be and the Primordial 7Li Problem

Emily E. Kading
University of Connecticut, emily.kading@uconn.edu

Calibration of CR-39 Nuclear Track Detectors with Alpha-Particles and Protons for a Measurement of Neutron Interactions with ^{7}Be and the Primordial ^{7}Li Problem

Emily Elizabeth Kading

B.S., University of Connecticut, 2014

A Thesis

Submitted in Partial Fulfillment of the

Requirements for the Degree of

Master of Science

At the

University of Connecticut

2017

APPROVAL PAGE

Masters of Science Thesis

Calibration of CR-39 Nuclear Track Detectors with Alpha-Particles and Protons for a Measurement of Neutron Interactions with ^{7}Be and the Primordial ^{7}Li Problem

Presented by

Emily Elizabeth Kading, B.S.

Major Advisor_____

Moshe Gai

Associate Advisor_____

Gerald Dunne

Associated Advisor_____

Peter Schweitzer

University of Connecticut

2017

Acknowledgments

First and foremost, I would like to sincerely thank my advisor Prof. Moshe Gai for the continuous support of my M.S. research work and for his motivation, patience, and immense knowledge of the subject. He taught me lifelong lessons in learning, research, and organization, all with an infectious joie de vivre. I could not have asked for a better mentor.

Besides my advisor, I would like to thank Prof. Aryeh Weiss at Bar Ilan University for his vast knowledge of microscopy image acquisition and image processing, as well as his patience in sharing some of this knowledge with me.

I would also like to thank Prof. Micha Hass, Dr. Shlomi Halfon, Dr. Leo Weissman, Dr. Dan Berkovits, Dr. Emilio Maugeri, and Dr. Thierry Stora for their invaluable guidance in research and for their insightful comments and hard questions.

Thank you to my advisory committee, Prof. Gerald Dunne and Prof. Peter Schweitzer, for their consideration, time, and important perspectives.

Finally, I would like to thank my parents, Elizabeth and James Kading, my brother Tristan Kading and my sister Charlotte Kading, and my grandparents Mary Lee and Michael Hannan, for their support throughout the process of writing my thesis and throughout my entire life.

Table of Contents

Abstract

The Primordial Lithium problem of Big Bang Nucleosynthesis (BBN), a prediction of ^{7}Li abundance which is considerably larger than observed, has important implications for the standard model of cosmology. Since ^{7}Li is produced by the later decay of ^{7}Be it is important to study the destruction of ^{7}Be during the epoch of BBN, in order to examine possible reduction of the predicted abundance of ^{7}Li, in particular the destruction of ^{7}Be with neutrons. The high flux of 50 keV epithermal neutrons (10^{10} n/sec/cm^2) produced by a Liquid Lithium (LiLiT) target at the Soreq Applied Research Accelerator Facility (SARAF) in Yavne, Israel offers opportunities for research at BBN energy. Due to the high intensity of the neutron flux at SARAF, background can be overwhelming for spectroscopic detectors.

The plastic polymer CR-39 (poly allyl diglycol carbonate - PADC, $C_{12}H_{18}O_7$) was chosen as a detector that can withstand the high neutron and associated gamma-ray flux. CR-39 Nuclear Track Detectors (NTD) have been calibrated for detection of alpha-particles and protons in a high neutron flux environment. These detectors can be used to detect damage caused by ionizing radiation on the plastic through a process of chemical etching. Charged particles leave behind a trademark path of chemical bonds broken by incoming ionized radiation. CR-39 is etched in a chemical bath of 6.25 N aqueous NaOH at 90^{o} C for 30 minutes. Etching is expedited along the track of radiation damage, as compared to the bulk etching of the plastic, and a micron-sized "pit" is revealed as a permanent record of the charged particle that caused the damage. Pits have different characteristics depending on the temperature and strength of the etching solution and amount of time the CR-39 spends immersed in the solution. An etching time of 30 minutes was chosen to distinguish the pits of alpha-particles from those of protons, which require several hours in the chemical bath to produce fully developed pits.

The pits on the CR-39 were imaged after etching using a camera attached to a microscope. Utilizing the motorized z-depth control of the microscope, a series of 11 images in 1.5 μm increments are taken around the plane of best focus. The images of the pits can then be analyzed using an automated segmentation algorithm that is capable of picking up pits above background noise and returns morphological information about individual pits. The images of the circular pits were digitally processed and the radii were extracted to allow for measurement of the charged particle type and energy.

CR-39s were irradiated by Rutherford backscattering of alpha-particles ranging in irradiation energies of 1.5 MeV to 9.5 MeV and protons of 1.4 MeV from a self-supporting thin 100 μg/cm^2 gold foil, along with alpha-particles from standard radioactive sources: ^{148}Gd (3.18 MeV), ^{241}Am (5.49 MeV), ^{228}Th (5.34-8.78 MeV). Background from reactions inside the CR-39 was calibrated using a cold neutron beam to measure the $^{17}O(n,\alpha)$ reaction that occurs inside of the CR-39 along with 2.2 MeV background gamma-ray. A radii region of interest (1.4-3.4 μm)

was determined for detection of alpha-particles in the desired energy range (1.5-3.5 MeV) to study the interaction of neutrons with ^{7}Be. The background reaction of ^{17}O(n,α)^{14}C that occurs within the CR-39 generates 1.4-1.7 MeV alpha-particles together with 0.6-0.3 MeV ^{14}C. The background pits created by these reactions are the limiting factor for the measurement of small cross-sections, as determined by the calibration process. The measurement of small cross-sections is the goal for understanding the destruction of ^{7}Be in the ^{7}Be(n,α) to further understand the Primordial Lithium problem.

I. INTRODUCTION

Big Bang Nucleosynthesis (BBN) [1–3] occurred between 1 second, when neutrons and protons fell out of equilibrium, to 10^3 seconds (20 minutes) after the Big Bang. This period was marked by rapid cooling and expansion, during which temperatures dropped from 1 MeV, when the neutron was no longer in equilibrium with the proton, to 30 keV, where freeze out of element production occurs. A few light nuclei other than hydrogen were formed during BBN: ^{4}He, deuterons, ^{3}He, ^{7}Li, and the unstable radioactive nuclei of ^{7}Be and ^{3}H. The one free parameter of BBN is the baryon/photon ratio which has now been measured with high precision by the Wilkinson Microwave Anisotropy Probe (WMAP) [4] and can now be used to predict the abundance of the light nuclei formed during BBN. The predicted abundances of ^{4}He, deuteron, and ^{3}He relative to hydrogen have been confirmed in good agreement with the observed high precision astronomical observations of old globular cluster stars. Measured abundance of ^{7}Li, however, is a factor of 3-4 below BBN prediction, as demonstrated below in Fig. 1. The cosmological implications of this problem make it an important issue to shed light on.

Examining the rates of BBN nuclear-reactions is crucial to better understand the circumstances of the Primordial Lithium problem [5]. Since ^{7}Li is the daughter isotope of ^{7}Be, the destruction rate of ^{7}Be with neutrons in the ^{7}Be(n,α)^{7}Li reaction and the ^{7}Be(n,$\gamma\alpha$) reaction influences the observed abundance of ^{7}Li in the early universe. If the destruction rate is increased, the abundance of ^{7}Li will be reduced. The destruction of ^{7}Be and formation of ^{7}Li occurred between the temperatures of 43-69 keV, which is highlighted in Fig. 2.

The Soreq Applied Research Accelerator Facility (SARAF) [6], at the Soreq Nuclear Research Center in Yavne, Israel, produces a high intensity ($\sim 10^{10}$ n/sec/cm^2) of epithermal $\sim$ 50 keV neutrons generated from the interaction of protons with a flowing Liquid Lithium target(LiLiT) [7, 8]. The neutron beams are produced in the ^{7}Li(p,n)^{7}Be reaction near threshold by bombarding LiLiT with a 1-2 mA proton beam for a total of 3.11 mA Hr with energy E_p = 1.935 MeV and energy spread of 15 keV. The resulting neutrons are confined to the forward angles (<60°) with a quasi-Maxwellian energy distribution [9, 10] with "effective temperature corresponding to the energy of kT = 49.5 keV. The quasi-Maxwellian

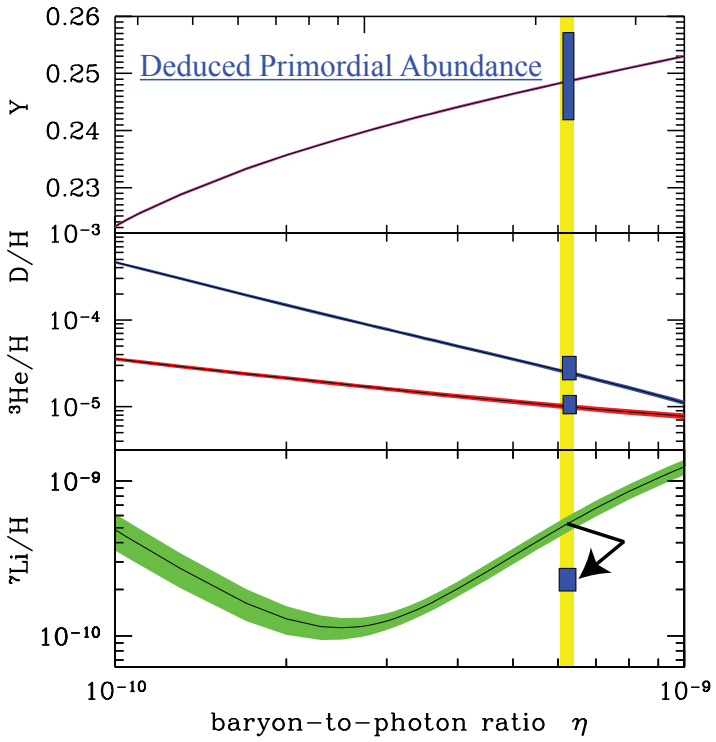

FIG. 1: The Primordial ^{7}Be problem: Observed Primordial Lithium abundance indicated in blue lies a factor of 3-4 below abundance predicted by the standard model. Abundances of ^{4}He, ^{2}H, ^{3}He lie in good agreement with standard model predictions. The volume of the baryon to photon ratio measured by WMAP is indicated in the yellow vertical band.

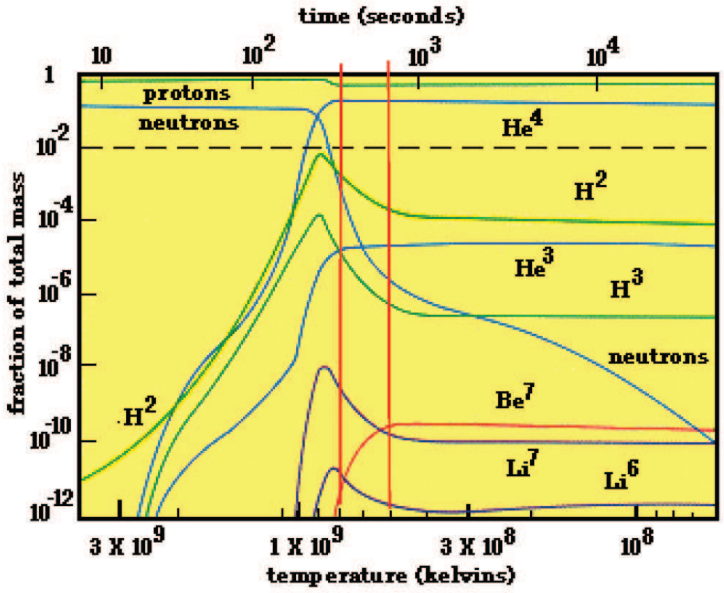

FIG. 2: The production of light nuclei during BBN as a function of time and temperature. The temperature range of interest for the ^{7}Be(n,α)^{7}Li is between 0.5-0.8 GK(43-69 keV).

energy distribution of the neutron beam with effective temperature corresponding to 49.5 keV presents opportunities to conduct research at the very same conditions as the epoch of BBN within the range of interest for studying the Primordial Lithium problem. However, the background created by the high intensity neutron flux with an associated flux of 477 keV gamma-rays ($\sim 10^{11}$ γ/sec) from the ^{7}Li(p,pγ) reaction, and 14.6, 17.6 MeV gamma-rays from the ^{7}Li(p,γ) reaction ($\sim 10^{9}$ γ/sec), along with gamma-rays produced by the interaction of neutrons with materials surrounding the target, causes difficulties for conventional spectroscopic systems such as silicon detectors.

We chose in this experiment [6, 7] to use CR-39 Nuclear Track Detectors (NTD) purchased from Homalite^{TM} for the detection of alpha-particles from the ^{7}Be(n,α) interaction. Accuracy in alpha-particle detection of the CR-39 was determined from the prototype "demonstratition of principle" measurement of the cross-section of the ^{10}B(n,α) reaction (with a fluence of 4.6 x 10^{9} neutrons) [13]. Charged particles impinging on the CR-39 break chemical bonds in the plastic, and these trails of damage become visible after being etched in NaOH, a caustic base. The trail of chemical bonds broken by the incoming radioactive particle is etched more rapidly by the NaOH than the bulk of the plastic. Using the microscopes shown in Fig. 3 one can then see the trail of damage, known as a "pit, with characteristics, including radius, dependent on the energy and type of the charged particle. Fig. 4 features two images showing both the depth of trail damage left by alpha-particles and typical circular pits as seen from above, each captured with the Atomic Force Microscope (AFM) shown in Fig. 3.

To use the CR-39 NTD for measuring alpha-particles emitted by the ^{7}Be(n,α) reaction, a series of calibration procedures had to be undertaken. CR-39 detectors were irradiated with alpha-particle and proton beams of varying energies within the energy region of interest for the ^{7}Be(n,α) reaction.

The ground state of ^{7}Be, $3/2^{-}$, is indicated in Fig. 5. Beryllium has 4 protons and 3 neutrons, with a neutron hole in $P_{\frac{3}{2}}$ shell. The s-wave interaction of neutron (spin of 1/2) with the Beryllium $3/2^{-}$ results in 1^{-} or 2^{-} states. The energy of the 1^{-} state at 19.4 MeV is far from the threshold (18.9 MeV) and it contributes very little. The 2^{-} state at 18.91 is only 10 keV above threshold and it dominates the s-wave interaction; however, due to

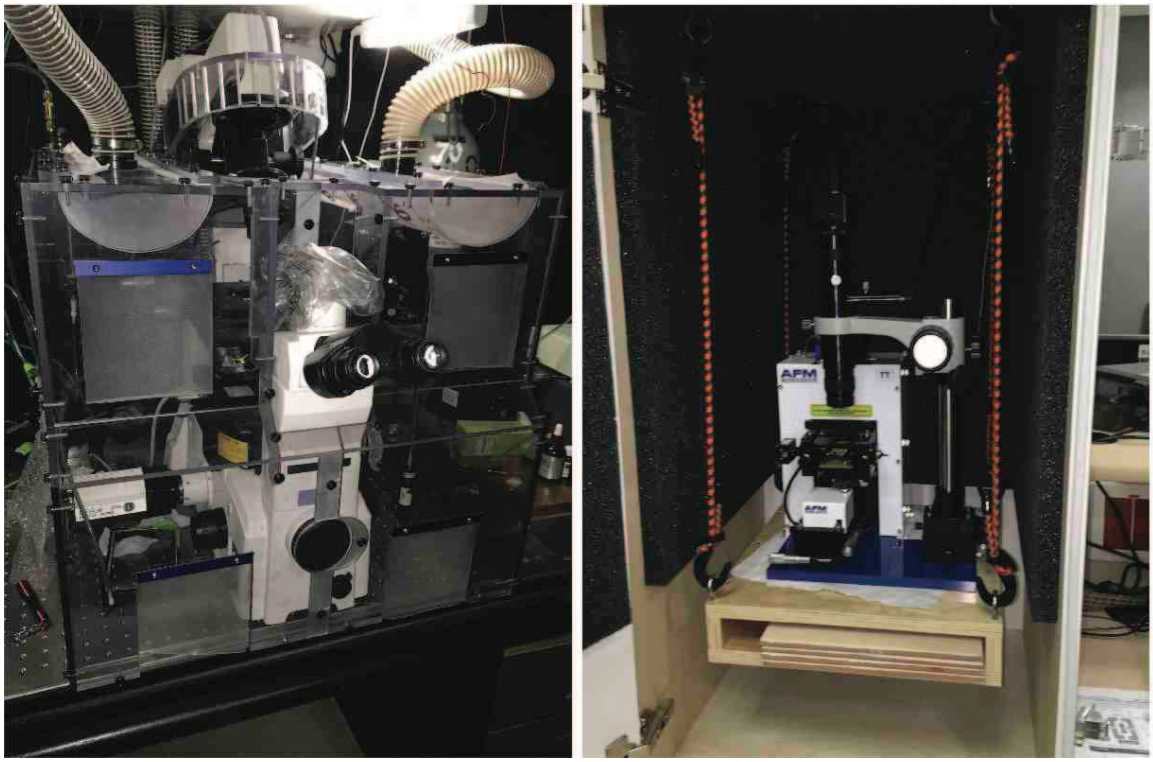

FIG. 3: The Nikon TE-2000E fully automated inverted microscope used for image acquisition (left) and the Atomic Force Microscope located at Bar Ilan University.

conservation of parity it cannot decay with alpha-particle emission. It instead decays with gamma-rays. Therefore, the energies we expect and calibrate the NTD for are alpha-particles of 9.5 Mev (degraded by aluminum foil to approximately 3.5 MeV), 8.4 MeV (degraded by aluminum foil to approximately 3.3 MeV) and 1.5 MeV (stopped) [11]. The energy region of interest for alpha-particles in the ^{7}Be(n,α) experiment is 1.5-3.5 MeV. The high energy alpha-particles($\sim$ 8.4 and 9.5 MeV expected from the ^{7}Be(n,$\gamma\alpha$) reaction and ^{7}Be(n,α) reaction, respectively, as shown in Fig. 5, are degraded with a 25 μm aluminum foil to energies $\sim$ 3.5 MeV.

The detectors were etched in a chemical bath of 6.25 N NaOH at 90° C for 30 minutes. The standardized etching conditions allow the comparison between pits of different irradiation particle types and energies. Freely available image processing software known as the Fiji [14] distribution of ImageJ [15], was used to develop a segmentation algorithm that could distinguish pits from background noise. Using the same algorithm on all detectors resulted in the establishment of a radius region of interest (RRI) for the pits of 1.5-3.4 μm. The

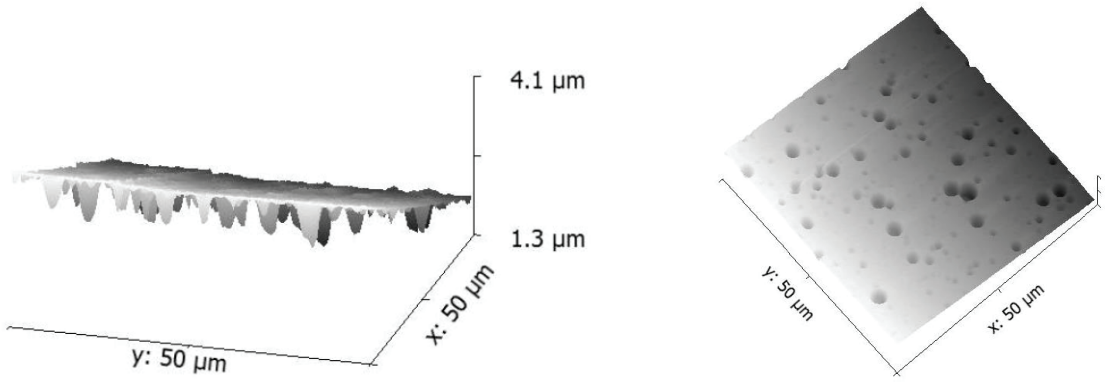

FIG. 4: Images taken by Atomic Force Microscope (AFM) of typical alpha-particle pits on a CR-39 NTD, shown from above as circular objects (right) and as a side profile as tracks penetrating the CR-39 (left).

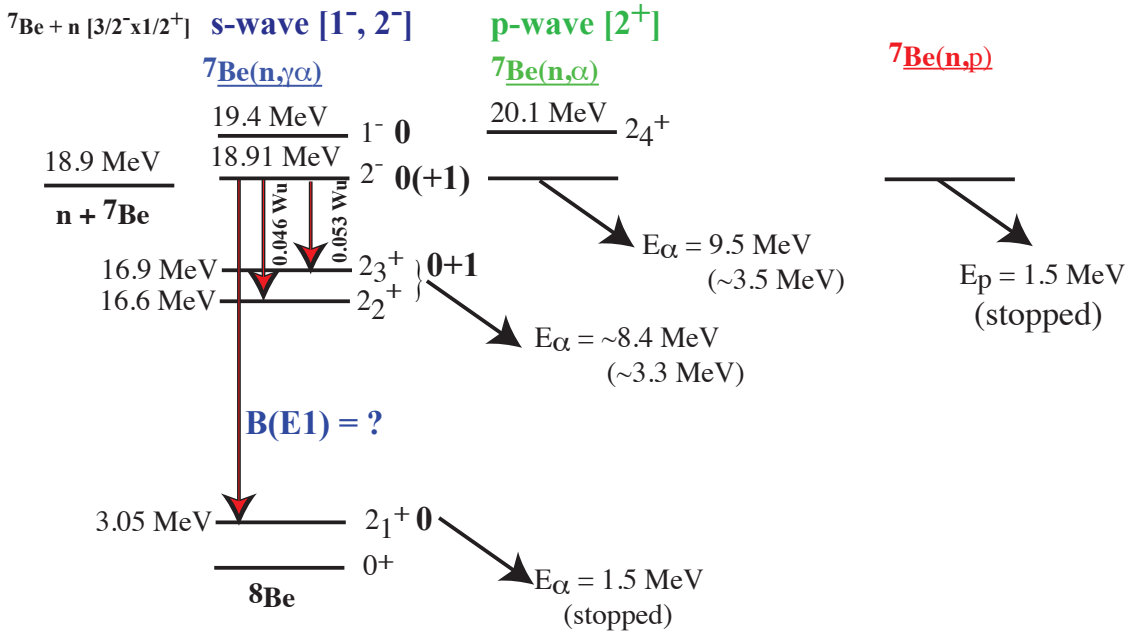

FIG. 5: The states in ^{8}Be that are involved in the s-wave (shown in blue) and p-wave (shown in green) interaction of neutrons with ^{7}Be and the charged particles from the decay of these states. In parenthesis we show the energy of the charged particles after traversing a 25 micron aluminum foil.

background produced in the neutron and gamma-ray rich environment was also studied using a ^{9}Be phantom target.

TABLE I: List of Reaction of Interest and Measured Byproducts

Interaction	^{7}Be(n,α)	^{7}Be(n,$\gamma\alpha$)	^{7}Be(n,p)	^{17}O(n,α)	Neutron-Scattering	Compton-Scattering
Type	signal	signal	backgrnd	backgrnd	backgrnd	backgrnd
Measured Product	α (degraded)	α (degraded), α	p	α + ^{14}C	n, p	γ, x-ray, e
Energy (MeV)	9.5 ($\sim$3.5)	$\sim$8.4 ($\sim$3.0), 1.5	1.4	1.4 + 0.6, 1.7 + 0.3	0.001 - 0.18	2.2, 0.477, 14.6, 17.6, 0.069
Calibration Source	^{148}Gd	VDG-RBS, ^{148}Gd	VDG-RBS	VDG-RBS, ILL(CN)	LiLiT, ^{9}Be(n,n)	ILL(CN), LiLiT, RBS

II. EXPERIMENTAL PROCEDURE

A. Calibration

To calibrate the CR-39 plates for use as detectors in the ^{7}Be(n,α) reaction, a series of irradiations of the NTD alpha-particles and protons were completed. At the TUNL tandem accelerator at Duke University, beams of 1.5-9.0 MeV alpha-particles irradiated the plates via Rutherford backscattering off a thin 100 μg/cm^2 gold foil. The setup is shown in Fig. 6; note also the presence of a silicon detector to calculate the efficiency of the CR-39 NTD. A further calibration of 1.5 MeV alpha-particles and 1.4 MeV protons was carried out with the 3 MV single ended van de Graff accelerator at the Weizmann Institute in Rehovot, Israel. The detectors were also calibrated with alpha-particles from standard sources: ^{148}Gd (3.18 MeV), ^{241}Am (5.49 MeV), and ^{228}Th (5.34-8.78 MeV).

The plates were etched in a standard 6.25 N NaOH aqueous solution heated on a hot plate to maintain a stable 90°C for 30 minutes. The CR-39s were mounted in the chemical bath in a custom made holder which kept them fully submerged in the solution and separate from each other during etching. This etching process results in circular, micron-sized pits which are visible by microscope. The bulk etch rate of the CR-39 was measured by weighing a non-irradiated CR-39 before and after etching. The rate was found to be relatively high, approx. 10 μm per hour, due to the high temperature of the NaOH.

The CR-39s were scanned preliminarily with a simple biological microscope at the Lab-

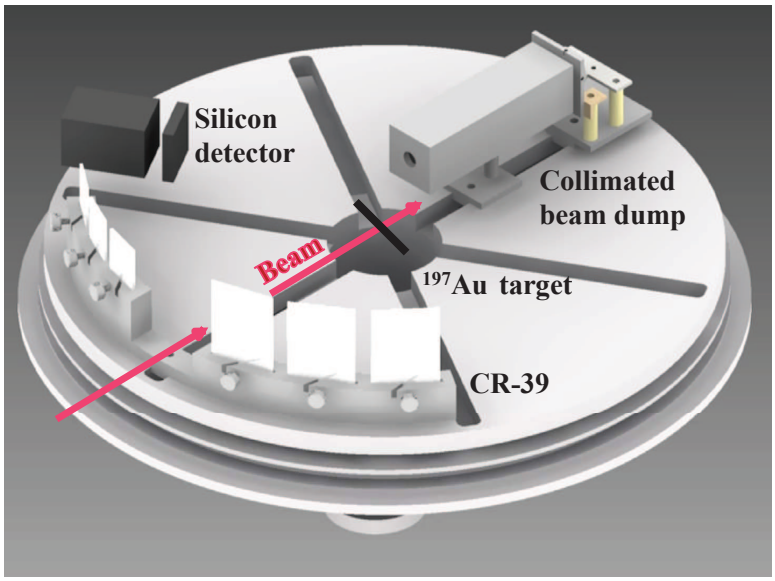

FIG. 6: Schematic diagram of the experimental setup used at the TUNL at Duke University and the 3 MV van de Graaff accelerator at the Weizmann Institute of Sciences.

oratory for Nuclear Science at UConn. Imaging of the etched CR-39 plates took place at Bar Ilan University in Ramat Gan, Israel with a Nikon TE-2000E fully automated inverted microscope (Fig. 3) set for brightfield imaging, controlled by NIS Elements software (version 4.3), through a 40X/NA = 0.6 LWD objective with correction collar set to zero cover-glass thickness. Images were acquired with a QImaging Retiga 2000R cooled 2MP CCD camera. Large areas (typically 2mm x 2mm), exceeding the field of view (FOV) of the objective were acquired by capturing multiple fields stitched together with a 10% overlap. At each FOV, stacks of 11 images with 1.5 micron inter-plane spacing (15 μm depth total) were taken centered around the best focus plane for the pits. Non-uniform illumination and fixed artifacts on the camera/microscope lens were corrected for by taking a background illumination image with no detector present. Subsequent image processing was done with the Fiji [14] distribution of ImageJ [15]. Image processing steps included:

1. Non-uniform illumination and fixed artifacts are corrected for by dividing the images of the pits by the background illumination image.
2. Image stacks are created with the background removed images. A minimum intensity Z-projection of the 11-image stacks was taken to optimize the segmentation process with more uniformly dark pits. At the best focus plane, the pits are seen as dark circular objects. However, due to the concave shape of the pits, there is a second focus

plane with a visible bright spot in the middle of the pit. By taking a minimum intensity Z-projection, the minimum pixel intensity [from 0(black) 255(white)] is chosen for the values on each of the 11 focus planes. A single image is generated from the combined minimum intensity pixels for each focus plane in the stack. Of note, the bright spot could be a useful characteristic to consider in future analysis of pits using CR-39.

3. Minimum intensity images are stitched together using the Grid/Collection plugin [16] that is part of the Fiji distribution. 10% overlap between frames during image acquistion is accounted for in the stitching process. By stitching the images together, large FOV of the CR-39 detector can be analyzed at one time using the segmentation algorithm.

4. To analyze the pits, images must be converted to binary black images with white pits, done in a process known as Thresholding. ImageJ and Fiji offer a variety of Thresholding algorithms for the analysis of data. To achieve the desired thresholding on the CR-39 detectors, the Threshold from Background function included with the BAR plugin collection [17] was used. Criteria selection for pits was:

   Pixel intensity more than two standard deviations above the estimated background mean.

   Minimum pit area of 45 pixels (1.57 μm^2 with 40x microscope lens), indicating a minimum radius of 0.7 μm.

   Minimum roundness and circularity of 0.3 and 0.2, respectively.

5. BioVoxxel Toolbox [18] extended particle analyzer filtered the thresholded binary images on size, roundness, and circularity requirements and provided measurements of a variety of morphological parameters, including area, perimeter, roundness, and circularity.

Typical 40x magnification calibration images are seen in Fig. 7 and Fig. 8: the first of alpha-particle pits from ^{148}Gd with energy of 3.18 MeV and the second pits from 1.4 MeV proton calibration (using RBS calibration). The observed pit radii spectra resulting from the analysis of the irradiations with alpha-particles is displayed in Fig. 7. Following etching conditions as described above, we note that the pits of the 3.18 MeV alpha-particles from ^{148}Gd source are centered around radii of 2.8 microns (Fig. 7). We also observed that the pits of 5.49 MeV alpha-particles (from ^{241}Am source) have a similar shape as those shown in Fig. 7, but the spectra is centered around the lower radius of 2.0 microns. It is well known that the trend of increase and decrease of measured radii as a function of energy is strictly dependent on etching conditions [19]. We also observed this trend for pits from the ^{228}Th alpha-source (5.34-8.78 MeV).

In Fig. 8 we show the spectra of pit radii from the 1.4 MeV proton calibration (via RBS). The radii for the proton pits range from the minimum threshold of 0.7 micron to 1.4 micron.

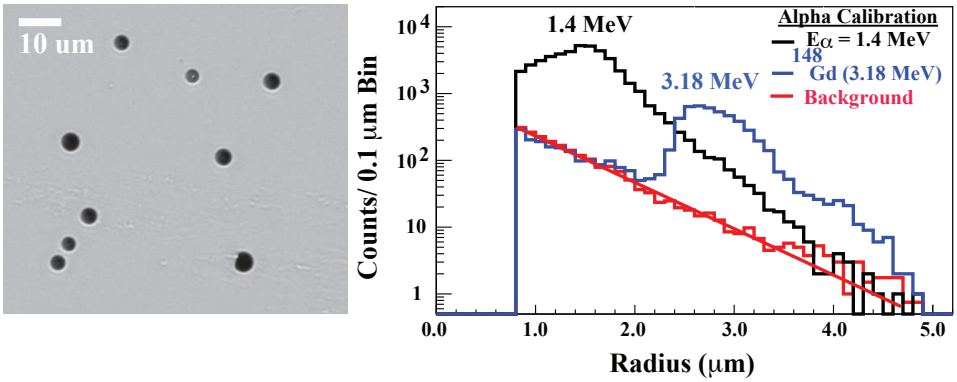

FIG. 7: Left: Typical pits observed after etching CR-39 plates exposed to 3.18 MeV alpha-particles from a ^{148}Gd source. A scale of 10 microns is shown. Right: The measured radii of pits in 6.7 mm^2 from irradiation with alpha-particles from a ^{148}Gd source (3.18 MeV) and RBS (1.4 MeV). The background shown of the ^{148}Gd source data was measured behind a thick aluminum foil that stopped the 3.18 MeV alpha-particles.

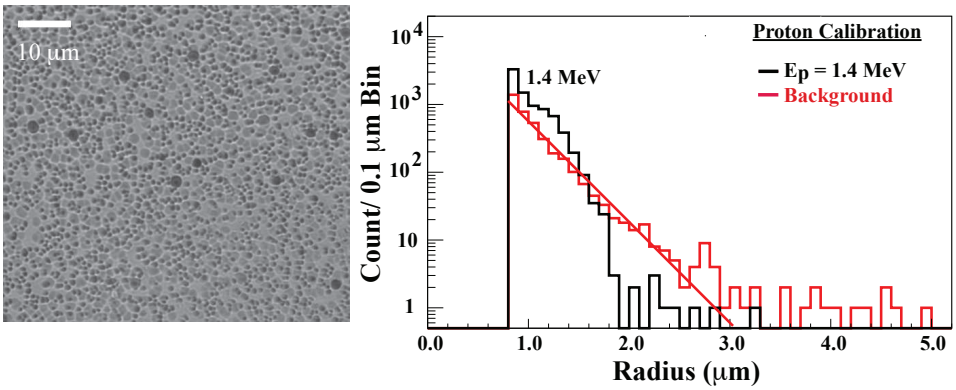

FIG. 8: Left: Typical pits observed for 1.4 MeV proton from the RBS calibration. A scale of 10 microns is shown. Right: The measured radii ($\sim$ 1.0 μm) of pits observed in 0.15 mm^2 from irradiation with protons. The background was measured behind a thick aluminum foil that stopped the protons.

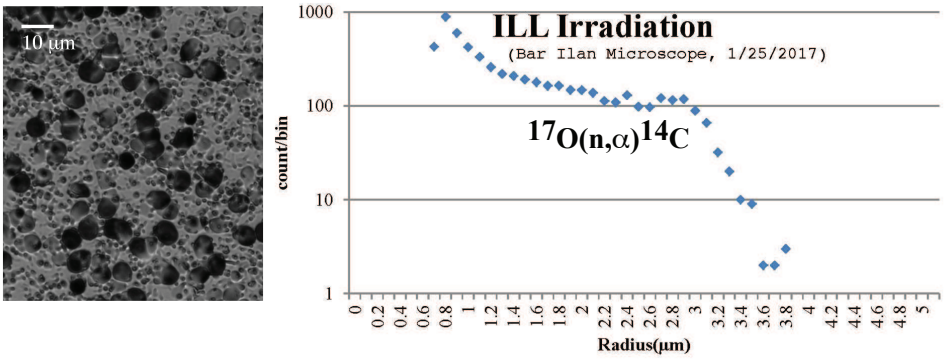

FIG. 9: Left: Typical pits observed with cold neutrons impinging on a bare CR-39 plate. A scale of 10 microns is shown. Right: The measured radii (1.4 - 3.4 μm) of pits observed in 1.9 mm^2 from 1.82 MeV deposited by α+^{14}C from the ^{17}O(n,α) reaction and Compton electrons ($<$ 1.0 μm) from the 2.2 MeV deuterium capture gamma-rays inside the CR-39 plate.

The CR-39s irradiated with protons undergo all of the same processing as the alpha-particle irradiated detectors. A standard etching time for irradiated plates at 90°C was determined by etching CR-39s in 10 minute intervals until we observed the expected number of fully developed pits for the well-known alpha-particle source activity, at 30 minutes total etching time. For the same 30 minute etching time, we observe only a fraction ($\sim$10%) of expected proton-pits calculated from the proton beam-target luminosity. The proton-pits that we do observe are not yet well developed and smaller in radii than the determined RRI for alpha-particles. Normally, etching times of several hours are used for proton irradiation [20]. By using a 30 minute etch time we are able to inhibit the development of proton pits to a region below 1.4 micron radii while allowing alpha-particle pits to fully develop.

The background spectra shown for the ^{148}Gd and proton calibrations in Fig. 7 and Fig. 8 were measured behind a 50μm aluminum foil which stopped the 3.18 MeV alpha-particles and 1.4 MeV protons. The measured background radii feature exponential behavior, although with different slopes, displayed by the straight lines on the semi-log plots. Backgrounds are found to be correlated with the dose of alpha-particles or protons. Every alpha-particle is associated with 40 keV x-rays of ^{144}Sm. Protons are associated with a larger flux of 69 keV x-ray of gold. The aluminum absorber does not stop these x-rays, they continue through to generate Compton electrons within the CR-39. It was observed that low energy electrons generate small radii pits [21], similar to the low radii and high density of the spectra displayed in Fig. 8. The low density of pits observed as background to the ^{148}Gd source shown in Fig. 7 allow us to conclude that the observed exponential behavior of background pits is not a matter of merged pits or an artifact of the analysis, but instead most likely produced by the Compton electrons. In Fig. 8, it is apparent that the background exceeds the proton spectrum above 2.0 micron radii, where the observed proton yield drops by a factor of more than a hundred. It is possible that we observe a sub-percentage contribution from x-ray produced by protons in the aluminum stopper foil.

Based on the calibration measurements shown in Fig. 7 and Fig. 8, we chose to define a conservative radii region of interest (RRI) for observing 1.5-3.5 MeV alpha-particles to be 1.4-3.4 microns. This RRI is well above the region where we observe an exponential rise in background pits (below 1.0 micron) and is also sufficiently higher than the radii of proton-

pits that extend to 1.4 micron radius. This conservative RRI does, however, result in a small portion of the alpha-pits to be missed at around 1.0 micron radii, which is incorporated into the calculation of total efficiency of the CR-39 plates.

Absolute detection efficiency of CR-39 NTD for detecting 3.18 MeV alpha-particles from a calibrated ^{148}Gd source (with absolute strength of$\pm$3.2%) was mesaured to be 93.3%$\pm$3.8%(stat) $\pm$3.2%(calibration) $\pm$3.5% (background and RRI). With a total uncertainty of 6.1%, we find the absolute detection efficiency of alpha-particle pits on the CR-39 is close to 100%. Additionally, a high resolution silicon detector measured alpha-particles from RBS with gold-foil within the TUNL measurement setup (Fig. 6) alongside the CR-39 detectors. The number of pits observed by the CR-39 detectors was found to be in good agreement with the measurement of the high resolution silicon detector from the RBS measurement.

B. Cold Neutrons Measurement

The ^{17}O(n,α)^{14}C reaction is a known source of background [22] when using CR-39 plates with neutrons, generating alpha-particles and ^{14}C within the CR-39 ($C_{12}H_{18}O_7$). To test this concept, a bare CR-39 NTD was irradiated with cold neutron beams at the Institute Lau Langevin (ILL) at Grenoble, France. These cold neutrons, below thermal energy at less than 25 meV, are not capable of breaking molecular bonds (obvious from the fact that CR-39 plastic is stable at room temperature). For this reason we can conclude that the CR-39 NTDs are not sensitive to direct cold neutron beam. The ILL cold neutron beam gamma-ray background is below the environmental ambient gamma-background. Therefore, no charged particles capable of producing tracks are present and any tracks found after etching the CR-39 must be produced by the interaction of cold neutrons with carbon, hydrogen, and oxygen. The ^{17}O(n,α) reaction and the H(n,γ) reaction are of particular interest, with large thermal cross section of 257 mb and 348 mb respectively.

The Q-value of the ^{17}O(n,α) reaction is 1.82 MeV, leading to a pencil sharp calibration line of 1.82 MeV deposited by the combined alpha-particle (1.41 MeV) and ^{14}C (0.41 MeV), as shown in Fig. 9. The observed signal from α+^{14}C is in excellent agreement with the RRI

of 1.4 - 3.4 micron determined by calibration measurements.

The thermal neutron cross section of the ^{17}O(n,α) reaction is known to be 257 mb, and the thermal equivalent total neutron fluence used in this measurement is 4×10^{14} n/cm^2. For the CR-39 area examined of 0.342 mm^2 we obtain a total cold neutron fluence of 1.36×10^{12} neutron. The molecular weight of CR-39 ($C_{12}H_{18}O_7$) is 274 g/mol with a density of 1.3 g/cm^3, hence a 1.0 micron thick layer of CR-39 contains 8×10^{14} ^{17}O /cm^2 (0.038% abundance). A 1.0 micron deep layer of CR-39 leads to 280 pits and the measured yield shown in Fig. 9 of 2466 pits implies a CR-39 fiducial volume approximately 8.8 microns deep. Therefore, we sample 8.8 microns of the CR-39 where nuclear tracks were produced inside the CR-39. Without claiming a quantitative understanding of pits within the CR-39, we instead note that the range of 1.41 MeV alpha-particles is 5.9 microns and the range of 0.41 MeV ^{14}C is 1.0 micron, hence the combined total length of the nuclear track of 6.9 microns is similar to our measured etch depth of approximately 5 microns. The deduced sampling depth of 8.8 microns appears to be within reasonable expectation based on the range and the depth of the etched CR-39. In conclusion, we find that the ILL measured pits in the RRI of 1.4 - 3.4 microns are due to nuclear tracks produced by the ^{17}O(n,α) reaction inside the CR-39.

C. The ^{9}Be "Phantom" Background

At SARAF, a ^{9}Be "phantom" target was bombarded with epithermal neutrons to measure background associated with the accelerator and the epithermal (49.5 keV) neutrons. In our measurements of high energy 8.4-9.5 MeV alpha-particles from a ^{7}Be target we do not observe substantial deviation from the measured background [11]. Therefore it is of interest to understand the source of the background in the in-beam measurement at SARAF with epithermal (49.5 keV) neutrons.

As discussed above, the spectrum measured at ILL for radii above 1.4 micron is in good agreement with the signal expected for the combined signal of α+^{14}C from the ^{17}O(n,α)^{14}C reaction inside the CR-39. The hydrogen to ^{17}O ratio in CR-39 is 6,770, hence in the ILL measurement we have 8700 H(n,γ)d captures for every ^{17}O(n,α) reaction with cross sections

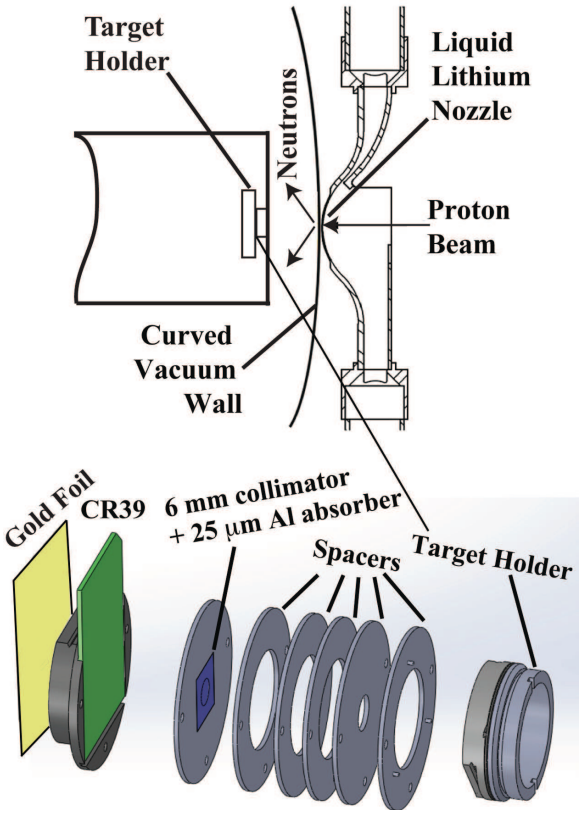

FIG. 10: Schematic diagram of the experimental setup used at SARAF.

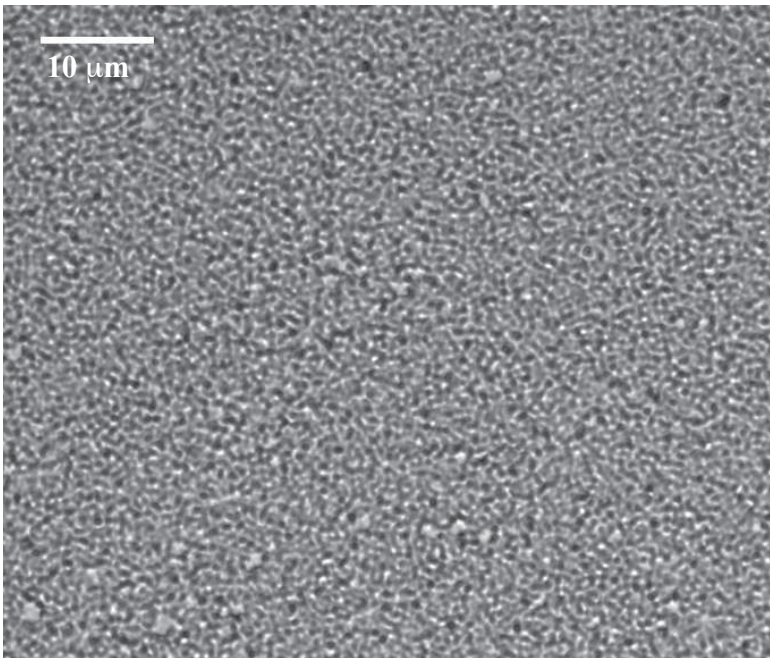

FIG. 11: Typical pits observed in-beam with neutrons impinging on the ^{9}Be target. The scale of 10 microns is shown.

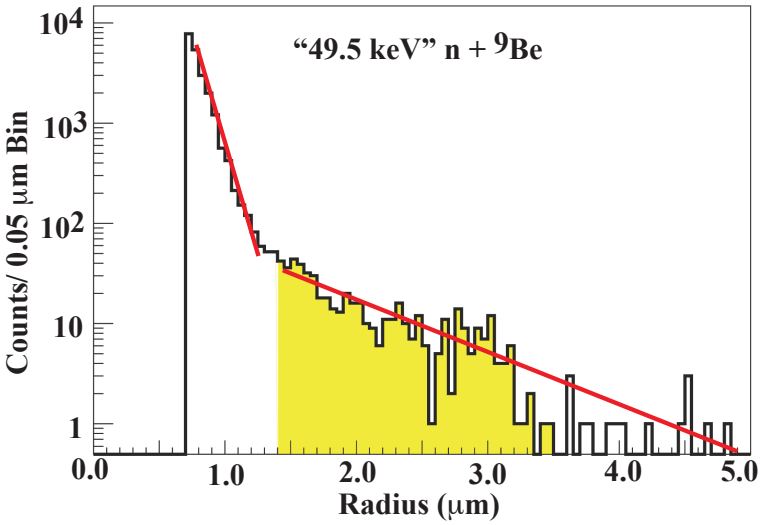

FIG. 12: The radii of pits measured over 16.36 mm^2 from the in-beam SARAF measurement with epithermal neutrons and ^{9}Be target. The radii region of interest (RRI) for alpha-particles (1.4 - 3.4 μm) is shown in hashed yellow.

of 348 mb and 257 mb, respectively. Hence a second major source of background in the cold neutron measurement are the 2.2 MeV gamma-rays of deuterium. The half length of 2.2 MeV gamma-rays in CR-39 is approximately 150 mm, hence we expect a substantial flux of high energy Compton electrons inside the 0.75 mm thick CR-39 plate. The pits with radii below 1.4 micron that exhibit an exponential rise toward low radii cannot be due to alpha-particles and we conclude they are due to the only remaining source of charged particles, namely electrons produced by the 2.2 MeV gamma-rays.

The interaction and hence pits from MeV gamma-rays and electrons in CR-39 is not well known, however as we discuss above low energy electrons were observed [21] to yield a high density of pits with very small radii. We observe the same high density of small radii in the cold neutron measurement, see Fig. 9. The proton calibration measurement shown in Fig. 8 exhibit similar high density of pits with small radii. As we discussed above the proton beam leads to a large flux of 69 keV x-rays from the gold foil. We conclude that the exponential rise at low radii observed in the cold neutron data and the proton calibration data is due to Compton electrons from high energy gamma-rays or x-rays.

D. Epithermal Neutrons (In-Beam) Measurement

An in-beam test of the CR-39 was performed at SARAF with the experimental setup shown in Fig. 10. The in-beam test was carried out with a ^{9}Be target in air, and it serves as a test benchmark for the ^{7}Be(n,α) measurement [11]. The neutron beams were produced by bombarding LiLiT [7, 8] with 1-2 mA proton beam for a total of 3.11 mA Hr with energy E_p = 1.935 MeV and energy spread of $\pm$15 keV. The resulting neutrons are confined to the forward angles ($\theta \leq 60^{\circ}$) with a quasi Maxwellian energy distribution [9, 10] with an "effective temperature" corresponding to the energy of kT = 49.5 keV. The integrated beam luminosity was measured with a fission chamber (not shown in Fig. 10) and by placing a gold foil directly behind the detector setup, as shown in Fig. 10, and then measuring the accumulated activity of the 412 keV line from the ^{197}Au(n,γ) reaction with a well known energy dependent cross section.

We used an 8 mm diameter ^{9}Be target prepared at the Paul Scherrer Institute (PSI) by electro-deposition on a 1.0 mm thick pure (99.999%) 5N aluminum backing [23]. The ^{9}Be target was enclosed on the front side with a 1.5 μm mylar foil, to reproduce the condition with the ^{7}Be target used for measuring the ^{7}Be(n,α) reaction [11]. In addition, a 25 micron pure 5N aluminum foil was placed in front of the CR-39 plates, as was done in the ^{7}Be(n,α) measurement [11] in order to stop the 1.4 MeV protons from the ^{7}Be(n,p) reaction (Table I).

The CR-39 NTD were placed behind a 6 mm diameter collimator made of 0.5 mm thick pure 5N aluminum that was placed at a distance of 7 mm from the ^{9}Be target (see Fig. 10). Areas smaller than 16.5 mm^2 (up to 4.6 mm diameter fiducial area) out of the available 28.3 mm^2 (6 mm diameter) were used to analyze pits in the NTD in order to stay clear of the edge of the collimator.

The CR-39 plates used in the in-beam measurement were etched and analyzed using the exact same procedure as for the calibration measurement. Fig. 11 is a typical image of the pits produced by the in-beam ^{9}Be target experiment, featuring a high density of small pits resembling the pit density observed in the proton calibration shown in Fig. 8 and the cold neutron measurement shown in Fig. 9. In Fig. 12 the radii spectrum results from this

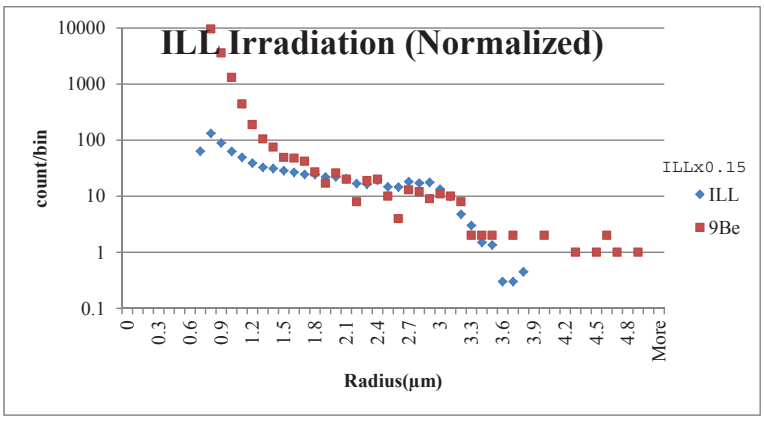

FIG. 13: Measurements of the background of cold neutron irradiation at ILL and ^{9}Be irradiation at SARAF plotted together. With a normalization factor of the ILL data multiplied by 0.15, the number of pits located in the RRI (1.4-3.4 μm) are in good agreement, leading us to conclude that this is the background data to expect in measurement of ^{7}Be(n,α) experiment.

experiment features an exponential rise in pits below 1.0 μm due to the Compton electrons from the intense 0.477, 14.6 and 17.6 MeV gamma flux produced by the LiLiT as well as "environmental" gamma rays produced by capture of neutrons on the surrounding materials (including the CR-39 itself). The RRI (1.4-3.4μm), hashed in yellow, deviates significantly from the exponential drop, and is dominated by pits produced by the ^{17}O(n,α) reaction. The results of the neutron beam on ^{9}Be target in air experiment will be our background for the ^{7}Be(n,α) and the ^{7}Be(n,$\gamma\alpha$) reactions [11].

E. Epithermal Neutrons (In-Beam) Results

In our attempt to understand the RRI shown in Fig. 12 we consider all possible neutron reactions with all materials included in the experimental setup shown in Fig. 10. We conclude that only the ^{17}O(n,α) reaction with Q-value = +1.82 MeV, and the ^{14}N(n,p) reaction with Q-value = +0.625 MeV, are energetically possible. The small amount of ^{14}N in the air, as well as our short (30 minutes) etching time, lead to a negligible background of proton-pits above 1.4 microns into the RRI of the alpha-pits. However the pits from the combined 1.4 - 1.7 MeV alpha-particles and 0.6 - 0.3 MeV ^{14}C from the ^{17}O(n,α)^{14}C reaction ($1 < E_n < 180$ kev), are a major source of background, as demonstrated in our cold neutron measurement discussed above. We note however, that in the case of cold neutrons the outgoing alpha-

particles and ^{14}C are mono-energetic (1.41 and 0.41 MeV, respectively), but in the case epithermal neutrons the outgoing alpha-particles and ^{14}C are emitted with a broad energy distribution due to the kinematics.

To calculate the ratio of the ^{9}Be irradiation with the cold neutron irradiation we must consider: the area ratio (16.36 mm^2 scanned for ^{9}Be, 0.342 mm^2 for cold neutron), the beam fluence ratio (4.99 x 10^{13} n/sec/cm^2 in ^{9}Be reaction, 4 x 10^{14} n/sec/cm^2 for cold neutron), and the cross-section of the ^{17}O(n,α) reactions in each experiment (3 mb for ^{9}Be, 257 mb for cold neutron). When these ratios are multiplied the result is a ratio of expected alpha-particles from ^{9}Be reaction to cold neutron reaction of 0.07 $\pm$0.03. In Fig. 13 we show comparison of the data normalized based on shape of spectra alone, with a normalization ratio of 0.15 $\pm$ 0.05. Thus, the background data observed is in agreement with our prediction based on the (very) different scanned areas, beam fluences, and cross-sections. This scaling again demonstrates that the observed background is from the ^{17}O(n,α) reaction inside the CR-39.

III. CONCLUSION

In conclusion, we calibrated CR-39 NTD with protons and alpha-particles of energies relevant to the reaction of ^{7}Be(n,α) to study the Primordial ^{7}Li problem of BBN, as shown in Figure 1 and Table 1. We studied with cold neutrons the background signal produced by reactions within the CR-39 by Compton electrons and ^{17}O(n,α). An etching process was developed to allow the full-development of alpha-particles while inhibiting the development of proton pits. Through calibration measurements, a RRI of 1.4-3.4 μm was determined for detection of alpha-particles of interest. We determined that this RRI is dominated by background pits produced by the ^{17}O(n,α) reaction occurring inside the CR-39. This background reaction is the limiting factor for determining low cross-section of the ^{7}Be(n,α). This measurement of alpha-particle emission rate is an important step in undering the

Primordial Lithium problem [11].

---

[1] D.N. Schramm and M.S. Turner; Rev. Mod. Phys. **70**, 303 (1998).

[2] S. Burles, K.M. Nollett and M.S. Turner, Astrophys J., **552**, L1 (2001).

[3] R. H. Cyburt, B. D. Fields, K. A. Olive, and T.-H. Yeh, Rev. Mod. Phys. **88**, 015004 (2016).

[4] J. Dunkley et al. (WMAP Collaboration), Astrophys. J. Supp **180**, 306 (2009).

[5] B. D. Fields, Ann. Rev. Nucl. Part. Sci. **61**, 47 (2011)

[6] A. Kreisel *et al.*, Proc. Linac 2014, Geneva, Aug. 31- Sept. 4, 2014, and WEIOB02 (2014) 770, http://accelconf.web.cern.ch/AccelConf/LINAC2014/ papers/weiob02.pdf.

[7] G. Feinberg, M. Paul, A. Arenshtam , D. Berkovits , D. Kijel, A. Nagler and I. Silverman, Nucl. Phys. **A827**, 590c (2009).

[8] S. Halfon *et al.*, Review Scient. Instr. **85**, 056105 (2014).

[9] G. Feinberg, M. Friedman, A. Krasa, A. Shor, Y. Eisen, D. Berkovits, D. Cohen, G. Giorginis, T. Hirsh, M. Paul, A.J.M. Plompen, and E. Tsuk, Phys. Rev. C **85**, 055810 (2012).

[10] M. Tessler *et al.*, Phys. Lett. **B751**, 418 (2015).

[11] E.E. Kading, M. Gai, T. Palchan, M. Paul , M. Tessler, A.Weiss, D. Berkovits, Sh. Halfon, D. Kijel, A. Kreisel, A. Shor, I. Silverman, L. Weissman, R. Dressler, S. Heinitz, E.A. Maugeri, D. Schumann, M. Hass, I. Mukul, Y. Shachar, Ch. Seiffert, Th. Stora, D. Ticehurst, C.R. Howell, N. Kivel, Bull. Amer. Phys. Soc. 61,13, 28 (2016).

[12] Dorothea Schumann, Massimo Barbagallo, Thierry Stora, Ulrich Kster, Moshe Gai, Nuclear Physics News, 26:4, 20 (2016).

[13] S. Halfon, M.Paul, A.Arenshtam, D.Berkovits, D.Cohen, I.Eliyahu, D.Kijel, I. Mardor, I. Silverman, Appl. Rad. Isotopes. **88**, 238 (2014).

[14] Johannes Schindelin, Ignacio Arganda-Carreras, Erwin Frise, Verena Kaynig, Mark Longair, Tobias Pietzsch, Stephan Preibisch, Curtis Rueden, Stephan Saalfeld, Benjamin Schmid, Jean-Yves Tinevez, Daniel James White, Volker Hartenstein, Kevin Eliceiri, Pavel Tomancak and Albert Cardona, Nature Methods **9(7)** 676 (2012)

[15] C.A. Schneider, W.S. Rasband, and K.W. Eliceiri, Nature methods **9(7)** 671 (2012). Google

Scholar: PMID 22930834.

[16] S. Preibisch, S. Saalfeld and P. Tomancak, Bioinformatics **25(11)**, 1463 (2009). Google Scholar: PMID 19346324

[17] T. Ferreira, K. Miura, B. Chef and J. Eglinger, Scripts: BAR 1.1.6, doi:10.5281/zenodo.28838, URL: https://doi.org/10.5281/zenodo.28838 (2015).

[18] J. Brocher, BioVoxxel Toolbox, 2014. [Online]. URL: http://fiji.sc/BioVoxxel_Toolbox. [Accessed: 13-Nov-2016].

[19] M. Sadowski, A. Szydlowski, M. Jaskola, T. Czyzewski, Rad. Measur. **28**, 207 (1997).

[20] N. Sinenian, M. J. Rosenberg, M. J.-E. Manuel, S. C. McDuffee, D. T. Casey, A.B. Zylstra, H. G. Rinderknecht, M. Gatu Johnson, F. H. Seguin, J. A. Frenje, C. K. Li and R. D. Petrasso, Rev. Sci. Instrum. **82**, 103303 (2011), with Erratum included.

[21] C.G.Wahl, J.G. McLean, Rad. Measur. **40**, 43 (2005).

[22] A. Seghour *et al.*, Nucl. Instr. Meth. Phys. Res. **A589**, 66 (2008).

[23] E.A. Maugeri, S. Heinitz, R. Dressler, M. Barbagallo, N. Kivel, D. Schumann, M. Ayranov, A. Musumarra, M. Gai, N. Colona, M. Paul, S. Halfon, and the n_TOF collaboration, Jour. Instr. **12**, P02016 (2017).

[24] P. E. Koehler and S. M. Graff, Phys. Rev. C **44**, 2788 (1991).